EFFECTS OF CALCIUM MISHANDLING IN ASTROCYTIC MITOCHONDRIA: THE UNEXPLORED POWERHOUSE

An Undergraduate Research Scholars Thesis

by

MEGAN HUANG FRAZIER[1], BELEN TORRES[2]

Submitted to the LAUNCH: Undergraduate Research office at
Texas A&M University
in partial fulfillment of requirements for the designation as an

UNDERGRADUATE RESEARCH SCHOLAR

Approved by
Faculty Research Advisor: Dr. Rahul Srinivasan

May 2021

Majors: Biomedical Sciences[1]
Genetics[2]

RESEARCH COMPLIANCE CERTIFICATION

Research activities involving the use of human subjects, vertebrate animals, and/or biohazards must be reviewed and approved by the appropriate Texas A&M University regulatory research committee (i.e., IRB, IACUC, IBC) before the activity can commence. This requirement applies to activities conducted at Texas A&M and to activities conducted at non-Texas A&M facilities or institutions. In both cases, students are responsible for working with the relevant Texas A&M research compliance program to ensure and document that all Texas A&M compliance obligations are met before the study begins.

We, Megan Huang Frazier and Belen Torres, certify that all research compliance requirements related to this Undergraduate Research Scholars thesis have been addressed with my Research Faculty Advisor prior to the collection of any data used in this final thesis submission.

This project required approval from the Texas A&M University Research Compliance & Biosafety office.

TAMU IRB: IBC2020-008 Approval Date: 06/09/2020 Expiration Date: 03/24/2023

TABLE OF CONTENTS

Page

ABSTRACT

Effects of Calcium Mishandling in Astrocytic Mitochondria: The Unexplored Powerhouse

Megan Huang Frazier[1], Belen Torres[2]
Department of Biomedical Sciences[1]
Department of Biochemistry and Biophysics[2]
Texas A&M University

Research Faculty Advisor: Dr. Rahul Srinivasan
Department of Neuroscience and Experimental Therapeutics
Texas A&M University

Astrocytes are the most populous cell type in the central nervous system (CNS) and are vital in neuron development, regulating blood flow, and maintaining communication between neurons. Astrocytic control on the CNS is due in part to their complex morphology, consisting of a circular soma extending into primary branches that further divide into smaller branchlets and leaflets. The morphology of astrocytes allows calcium (Ca^{2+}) to function as their main communicator, much like electrical signals in neurons. Increased Ca^{2+} in astrocytes causes gliotransmitter release, leading to regulation of synaptic transmission in neurons. The majority of Ca^{2+} signals in astrocytes originate in mitochondria, even within the nanometer sized branchlets and leaflets. Recent studies show Ca^{2+} mishandling in neuronal mitochondria leads to dysfunction and is associated with early neurodegeneration in Alzheimer's and Parkinson's disease. However, effects of Ca^{2+} mishandling in astrocytic mitochondria are less understood. Considering this, we will disrupt Ca^{2+} signaling specifically in astrocytic mitochondria using an adeno-associated virus (AAV) overexpressing neuronal Ca^{2+} sensor 1 (NCS1), a ubiquitous Ca^{2+}

buffering protein. Under normal conditions, NCS1 functions in neurotransmitter release, cell growth and survival. However, NCS1 is upregulated in schizophrenia, bipolar disorder, and autism as well as Parkinson's disease. In order to verify disruption of Ca^{2+} signaling via NCS1, our construct will first be assessed in the astrocytoma cell line, SMA-560. By assessing changes in morphology and respiration, as a result of Ca^{2+} mishandling, we hope to progress our understanding of the role this unexplored powerhouse plays in neurodegenerative diseases.

ACKNOWLEDGEMENTS

Contributors

We would like to thank our faculty advisor, Dr. Rahul Srinivasan and our graduate student, Taylor Huntington, for their guidance and support throughout the course of this research. We would also like to thank Eric Bancroft for his help maintaining our cell line.

Thanks also go to our friends and colleagues and the department faculty and staff for making our time at Texas A&M University a great experience.

The Seahorse XFe96 Analyzer used for mitochondria respiration was provided by COM-CAF. The analysis depicted in MitoGraph was conducted in part by Megan C. Harwig and was published in 2018. The Confocal microscope provided by the Texas A&M College of Medicine was used for imaging.

All other work conducted for the thesis was completed by the student independently.

Funding Sources

This research did not receive funding.

1. INTRODUCTION

Astrocytes are five times more abundant in the brain than neurons and were thought to only be the glue that holds neurons together, but in recent decades, they have been shown to perform a wide variety of brain processes. [1] We now know astrocytes play a role in cell fate determination, neuroinflammation, neuronal protection and neurogenesis. [2,3] They are essential for maintaining synaptic transmission, blood flow in the brain, and for producing neurotropic molecules important for developing and sustaining neurons. [4]

Astrocytes have a complex, ramified morphology consisting of a small soma, with thick, primary branches that give rise to branchlets and leaflets, collectivity known as primary astrocytic processes (PAPs). [5] It is the PAPs that interact with surrounding cells, including neurons and their synapses. [5] The nanometer sized PAPs allow for a high surface area to volume ratio. This enables astrocytes to contact synapses, blood vessels and other glial cells where they mediate multiple active and homeostatic roles. [6,7]

In order to contact and interact with other cells using these PAPs, Ca^{2+} plays an essential role in the astrocytic communication process. Astrocytes utilize Ca^{2+} in order to transmit and receive signals from neighboring neurons and other glial cells. Ca^{2+} activity in astrocyte branchlets release gliotransmitters, which play a role in modulating synaptic activity due in part to the incoming excitatory or inhibitory signals from surrounding cell. [8,9,10] These signals can cause integration and propagation of Ca^{2+} through the astrocyte network to allow communication between neurons. [9]

Ca^{2+} is not only important in astrocytes, but also utilized in astrocytic organelles, specifically the mitochondria. Mitochondrial Ca^{2+} plays pivotal roles in physiological processes

such as neuronal homeostasis, ATP production and induction of apoptosis. [11] Ca^{2+} enters the astrocyte through the plasma membrane. Ca^{2+} then makes its way into the cytosol or integrating itself into astrocytic organelles. The Golgi apparatus and endoplasmic reticulum release Ca^{2+} to be taken up by the mitochondria through the voltage-dependent anion channels (VDAC) on the outer membrane. Ca^{2+} then travels through the mitochondrial Ca^{2+} uniporter (MCU) on the inner membrane to the mitochondrial matrix. [12] Other channels that can pump Ca^{2+} into mitochondria include the Na^{+}/Ca^{2+} exchanger (NCX), and the $H+/Ca^{2+}$ exchanger (HCX). [13]

Mitochondrial Ca^{2+} is essential to astrocytes; however, in dysfunctional states, it is involved in various pathophysiological processes including inflammation and neurodegeneration. [12] Moreover, Ca^{2+} dysregulation can lead to a decline in mitochondrial function such as diminishing respiration and increasing reactive oxygen species. [14] Ultimately, mitochondrial Ca^{2+} dysfunction causes apoptosis, autophagy, and necrosis, which are observed in Parkinson's and Alzheimer's disease. [12,14] When aberrant Ca^{2+} signals are observed, an increased number of reactive astrocytes can be seen in the dorsolateral striatum (DLS) and hippocampus (HPC). [15] Mitochondrial Ca^{2+} dysfunction has been linked to early stages of neurodegenerative diseases and has been widely studied in neurons, but it has not been studied in the most populous cell type, astrocytes. Therefore, we will mishandle Ca^{2+} in mitochondria by upregulating NCS1 to observe changes in astrocytic health.

To better understand the role Ca^{2+} plays in astrocytic mitochondria, NCS1, a Ca^{2+} buffering protein, will be overexpressed in order to disrupt the normal Ca^{2+} concentration within astrocytic mitochondria. In standard conditions, NCS1 plays a vital role in neuronal functions including neurotransmission, survival, and plasticity. [16, 17] When NCS1 binds to Ca^{2+}, the mitochondria must make up for the loss and allow more Ca^{2+} entry. This creates an

overcompensation of Ca^{2+} leading to neurodegeneration. In neurodegenerative diseases, such as schizophrenia and bipolar disorders, thus, an increase in NCS1 levels is detected. [18]

The astrocytoma cell line, SMA-560, will be utilized in order to verify Ca^{2+} dysfunction via upregulation of NCS1 because of their fast growth rate. This project will be focused on observing changes in mitochondrial morphology and respiration, using MitoGraph and the Seahorse XFe96 Analyzer, respectively. By disrupting Ca^{2+} signaling, we hope to further our understanding of the role astrocytic mitochondrial Ca^{2+} play in neurodegenerative diseases.

2. METHODS

2.1 SMA-560 cells Care and Maintenance

2.1.1 Cell Splitting

The SMA-560 cells were maintained in a T-150 flask with complete media: Improved MEM media (Gibco, 10373-017) supplemented with 5% HI FBS (Gibco, 16140-063), an antimycotic – penstrep mix, ampicillin, and kanamycin. Cells were split when grown to 80-90% confluency. The cells were split into 96-well plates for the Seahorse XFe96 analysis and split onto circular coverglass slips for imaging and MitoGraph analysis. Cell splitting was done by aspirating old media from the flasks, rinsing 2x with serum free Improved MEM media, and incubated with accutase (Gibco, A1110501) at 37°C to detach cells from the bottom of the flask. Cells were then transferred to a 15 mL conical tube. The remaining cells in the flask were washed with complete media and added to the 15 mL conical tube and spun down in the centrifuge for 5 min at 900 xg. The supernatant was aspirated and complete media added to the conical tube to resuspend the pellet. Cells were then counted using a hemocytometer. Cell dilutions were made for MitoGraph analysis or Seahorse XFe96 Analysis and the remaining 5 million cells plated again in the original T-150.

2.1.2 Cell Plating

Two round, glass coverslips were added to each dish, filled with 70% ethanol and decontaminated under UV light. The remaining ethanol was aspirated and 100 μL of poly-L-lysine was added to each coverslip. Dishes were lightly agitated and put in the 37°C incubator overnight. Poly-L-lysine was aspirated, washed with MilliQ water and the desired number of

cells were distributed to each coverslip. After an hour, 2 mL complete media was added to each dish.

2.2 Infection of SMA-560 cells

2.2.1 Adeno-Associated Viral Vectors (AAVs)

The AAV 2/5 GfaABC$_1$D-mito7-eGFP and AAV 2/5 GfaABC$_1$D-mito7 -NCS1 constructs were created by Vector Builder (Chicago, IL) using the Gateway cloning method. GfaABC1D is an astrocyte specific promotor (877 bp). The mito7 (87 bp) will direct eGFP and NCS1 to the mitochondrial matrix. The GfaABC$_1$D-mito7-eGFP and GfaABC$_1$D-mito7 -NCS1 cassettes were introduced into a pZac2.1 plasmid. The pZac2.1 GfaABC$_1$D-mito7-eGFP and pZac2.1 GfaABC$_1$D-mito7 -NCS1 plasmids were used to generate AAV2/5 GfaABC$_1$D-mito7-eGFP and AAV 2/5 GfaABC$_1$D-mito7 -NCS1 viral vectors. [19]

2.2.2 Process of Infecting

SMA-560 cells were infected with AAV2/5 GfaABC$_1$D-mito7-eGFP as the control as well as a co-infection with AAV2/5 GfaABC$_1$D-mito7-NCS1 for NCS1 overexpressing cells. Several experiments were conducted with a range of viral titers in order to make sure cells were not over-infected or under-infected. The optimal viral titer chosen was 9.76 x10^{12} GC/mL for AAV2/5 GfaABC$_1$D-mito7-eGFPand a matched viral titer for AAV2/5 GfaABC$_1$D-mito7-NCS1. To infect the SMA-560 cells, dishes were washed with serum free Improved MEM media. A master mix containing AAV2/5 GfaABC$_1$D-mito7-eGFP, and when needed AAV2/5 GfaABC$_1$D-mito7-NCS1 virus, in 2.5 mL of serum free Improved MEM media was added to each dish and incubated for an hour. After the 1 hr incubation period at 37°C, 2 mL of complete

media was added to each dish. To efficiently infect the SMA-560 cells, cells were incubated for 48 hours before experiments.

2.2.3 Fixing Cells

After infection for 48 hours complete media was aspirated, and 2 mL of 10% formalin were added to each dish and cells gently agitated for 20 min. The cells were then washed twice with 2 mL of PBS each for 5 min with slow agitation. Finally, cells were mounted to glass slides (North American, 48300-025) using Fluoromount (Diagnostic BioSystems, K024).

2.3 Mitochondrial Respiration

2.3.1 Infection

In order to infect enough cells needed for Seahorse analysis, a mass infection was utilized. The SMA-560 cells were split from a T150 flask (Corning, 3291) and 200,000 cells each were seeded into 4 separate T25 flasks (Corning, 3289). Cells were allowed to grow for 48 hrs before infection. NCS1 cells were infected with 2.44×10^{10} genomic copies (GC) of AAV 2/5 GfaABC$_1$D-mito-7-NCS1. Cells were allowed to grow for 48 hrs after infection before being plated in the Seahorse.

2.3.2 Mito Stress Test Kit

The Seahorse XFe96 Analyzer (Agilent Technologies, Santa Clara, CA, USA) measures glycolytic and mitochondrial respiration. The Mito Stress Test Kit (Agilent Technologies, 103708-100) was utilized in order to specifically measure oxygen consumption rate (OCR) in pmol/min and extracellular acidification rate (ECAR) in mpH/min. After 48-hr infection with or

without NCS1, cells were plated at 50,000 cells/well in the Seahorse XF Cell Culture Microplate (Agilent Technologies) in complete media. The sensor cartridge was hydrated with 200 µL Seahorse XF Calibrant (Agilent Technologies) at 37°C in a non-CO_2 incubator overnight. All wells in the plate were hydrated. The plate map was then designed in Wave software (Agilent Technologies).

Seahorse assay media was prepared by supplementing Seahorse XF DMEM medium with 1 mM pyruvate, 2 mM glutamine, and 10 mM glucose (Agilent Technologies, 103708-100) and pre-warmed to 37°C in a water bath. The concentrations of compound stock solutions were 100 µM oligomycin, 100 µM carbonyl cyanide-4-phenylhydrazone (FCCP), and 50 µM rotenone/antimycin A. Final inhibitor concentrations were 1.5 µM, 1.0 µM, 0.5 µM for oligomycin, FCCP, and rotenone/antimycin A, respectively.

The Wave Program was used to design the plate map and analyze results. A plate map was utilized to assign groups to calculate group statistics for measurements performed. [20] To analyze the final results, data was exported into Microsoft Excel. A single-file summary report was generated, giving the following measurements for OCR and ECAR: basal respiration, ATP production, proton leak, maximal respiration, spare capacity, and non-mitochondrial oxygen consumption.

2.3.3 Analysis

Oxygen consumption rate (OCR) and extracellular acidification rate (ECAR) were measured on the Seahorse XFe96 Analyzer. OCR is the amount of oxygen being consumed in pmol/min and ECAR is an indicator of pH change. OCR and ECAR are indirect measurements of the amount of ATP in the mitochondria.

The following measurements are automatically generated using the single-file report summary for the MitoStress Test. Basal respiration gives a baseline measurement of the oxygen being consumed under normal, physiological conditions. ATP production indicates the amount of ATP being produced, solely by the electron transport chain (ETC). Proton leak is a measurement of how much ATP is being produced outside of the ETC. Maximal respiration shows the maximal amount of ATP the mitochondria can produce. At the same time, spare respiratory capacity measurements are taken, indicating how much ATP is produced in order to compensate for the cell's needs. Non-mitochondrial oxygen consumption gives a measurement of how much ATP is being produced outside of the mitochondria.

2.4 Mitochondrial Morphology

2.2.1 Image Acquisition

Images were taken using a FV 1200 inverted Olympus confocal microscope equipped with a 60x oil objective (NA 0.8) and 488, 561 nm laser lines. All images were acquired using the same conditions: 60X 3X magnification, 550 HV, 2x Gain, 5% laser, and 0% offset along with a small z-spacing (0.2 um). Astrocytes were chosen if they were semi-isolated and mostly separate from adjacent astrocytes.

2.2.2 Image Analysis

MitoGraph 3.0 is an open-source, C++ program that processes images and creates three-dimensional (3D) mitochondrial structures. [21] The MitoGraph software can be found online (https://github.com/vianamp/MitoGraph). In order to obtain quantifiable data of astrocytic mitochondrial morphology, MitoGraph 3.0 was used to acquire data from confocal imaging. MitoGraph was downloaded and saved to a desktop folder for later use. MitoGraph was operated

through a Mac terminal. Before running MitoGraph, the terminal directory was directed to the folder containing MitoGraph using the command (cd ~/Desktop/MitoGraph) . The file was made executable using the command (chmod +xxx MitoGraph). [21] All of the images were processed through MitoGraph using the following command (./MitoGraph -xy 0.138 -z 0.2 -scales 1.1 1.4 4 -adaptive 10 -path ~/Desktop/Images/cells). The parameters were optimized for SMA-560 cells. The z-stack images were converted into maximum intensity z-projections using FIJI (Images -> Stacks -> Z project). [21] Once all of the images were converted into maximum intensity z-projections the images were then converted to TIFF files. All of the images and TIFF files were added to the same desktop folder.

First, the GenMaxProjsFrom.ijm macro was directed to run on the desktop file containing the original images and the TIFF files. GenMaxProjsFrom.ijm creates maximum intensity projections for all of the images in the dataset. The resulting file was saved as MaxProjs.tif and in the same file with the other images. A single ROI was drawn around each cell using the MaxProjs.tif stack. The next macro, CropCells.ijm, uses the ROIs and crops the original images to create a new 3D image file containing a single cell which will be used in the MitoGraph software. Before running the CropCells.ijm macro it had to be modified to fit the image parameters for larger astrocyte cells. The changes were as follows, in the script for CropCells.ijm find "//Defining the size of the single cell images:_xy = 200" and replace 200 with 512. The second change made to the macro was adding "//" before "run("Add Specified Noise...", "slice standard=" + 0.5*std);". [21] The ROIs were saved as RoiSet.zip and added to the same folder with the MaxProjs.tif and the TIFF files. The CropCells.ijm macro was then set to run on the desktop folder containing the RoiSet.zip file, MaxProjs.tif and TIFF files. Once completed, a new folder was created called 'cells' which contained all of the cropped images. After running

MitoGraph, the PNG images were examined to ensure that the entire mitochondrial network mirrored the original confocal images.

There were two R-scripts used to process the numerical data provided from MitoGraph: CreateSummary.R and CreatePlots.R. These R-scripts can be found online (https://github.com/Hill-Lab/MitoGraph-Contrib-RScripts.git). First, R and R-studio were downloaded and placed them in the folder containing all of the MitoGraph output files. In R-studio the two R-scripts were opened and the directions at the top of the scripts were followed. The files generated were used to quantify astrocytic mitochondrial morphology.

3. RESULTS

3.1 Seahorse XFe96 Analyzer: Mito Stress Test Kit

Table 1. Mito Stress Test Kit results. 50,000 cells/well with control and 50,000 cells with NCS1. Results are averages from three measurements and include the standard error of the mean (SEM).

	Drug Injected	Control	NCS1	Change with NCS1
Non-Mitochondrial Oxygen Consumption (pmol/min)	-	41.23 ± 1.44	37.95 ± 3.08	No change
Basal Respiration (pmol/min)	-	142.76 ± 10.05	182.89 ± 11.04	Increase
Proton Leak (pmol/min)	Oligomycin	57.18 ± 9.13	53.57 ± 4.41	No change
ATP Production (pmol/min)	Oligomycin	85.58 ± 12.15	129.32 ± 9.23	Increase
Maximal Respiration (pmol/min)	FCCP	236.67 ± 18.13	251.94 ± 13.27	Increase
Spare Respiratory Capacity (pmol/min)	Rotenone/Antimycin A	93.91 ± 14.61	69.05 ± 10.11	Decrease
Spare Respiratory Capacity (%)	Rotenone/Antimycin A	173.08% ± 9.81%	147.52% ± 6.26%	Decrease
Coupling Efficiency (%)	-	55.48% ± 6.73%	69.92% ± 2.74%	Increase

Before final experiments were ran, an FCCP titration with a variety of cell densities experiment was ran. This was done in order to determine which FCCP concentrations and cell densities worked best with the SMA-560 cells. To determine FCCP titrations and cell densities, initial experiments were ran with FCCP concentrations at 0.125 µM, 0.25 µM, 0.5 µM, 1.0 µM, and 2.0 µM. Cell densities were ranging from 10,000 cells/well to 50,000 cells/well in increments of 10,000. 50,000 cells/well and an FCCP concentration of 1.0 µM gave consistent measurements and was determined as best fit for Seahorse experiments.

Basal respiration results comparing the control cells to the NCS1 infected cells showed a significant 1-fold increase (Mann-Whitney t-test, $p = 0.007$) (Table 1, Figure 1.1). This data was taken before any injections, indicating the starting oxygen consumption rate (OCR). Once oligomycin (inhibitor of complex V) was injected, the OCR had a significant, 1-fold increase (student's t-test, $p = 0.005$) in NCS1 cells compared to control cells (Table 1, Figure 1.5). There was no change (Mann-Whitney t-test, $p = 0.137$) in proton leak of NCS1 cells (Table 1). The FCCP injection (inhibitor of complex IV) led to maximal respiration, which showed a slight increase (Mann-Whitney t-test, $p = 0.499$) in NCS1 cells (Table 1). Rotenone/Antimycin A was injected, leading to a decrease in spare respiratory capacity (Mann-Whitney t-test, $p = 0.125$) (Table 1). The non-mitochondrial oxygen consumption showed no change between control and NCS1 cells (Mann-Whitney t-test, $p = 0.499$) (Table 1). The coupling efficiency showed a slight increase with NCS1 injections (Mann-Whitney t-test, $p = 0.119$) (Table 1).

Figure 1.1. Basal Respiration

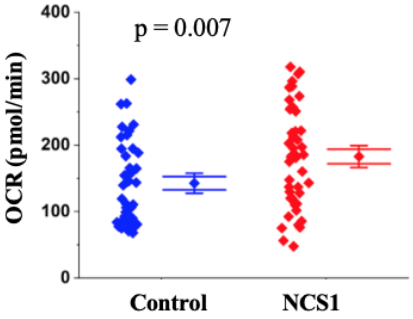

Figure 1.2. Non-Mitochondrial Oxygen Consumption

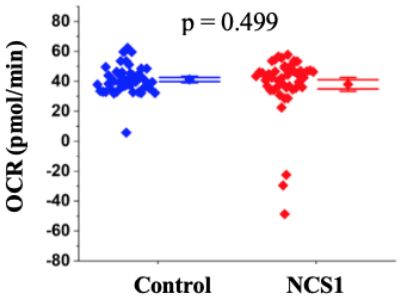

Figure 1.3. Maximal Respiration

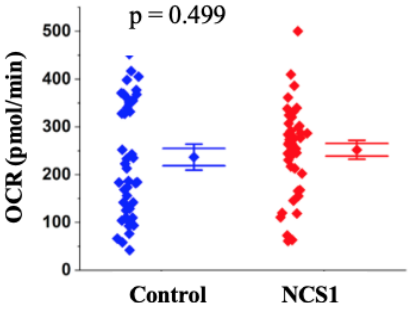

Figure 1.4. Proton Leak

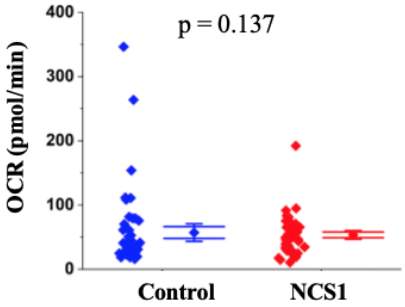

Figure 1.5. ATP Production

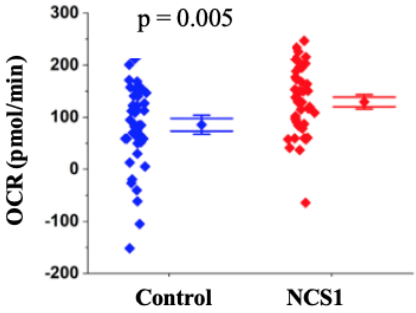

Figure 1.6. Spare Respiratory Capacity

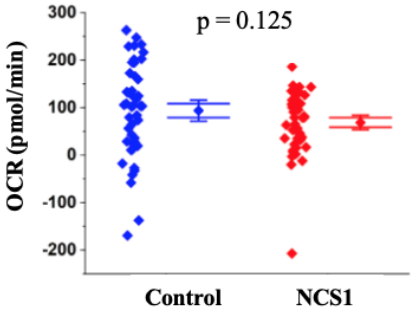

Figure 1.7. Spare Respiratory Capacity (%)

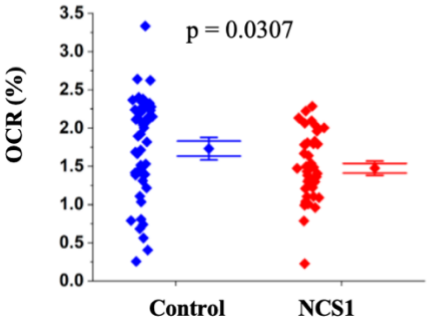

Figure 1.8. Coupling Efficiency

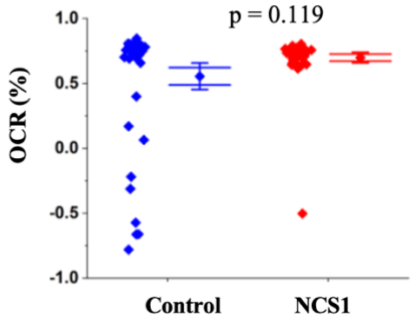

Figure 1. Graphs comparing Mito Stress Test parameters in control conditions and NCS1 conditions. The following are parameters being measured in the Seahorse XFe96 Analyzer.

3.2 Quantifying the Mitochondrial Network

In order to acquire quantifiable images of mitochondrial morphology in SMA-560 cells, we imaged 50,000 cells/coverslip. In order to visualize changes associated with overexpression of NCS1 we will be using an AAV 2/5 GfaABC$_1$D-mito-7-NCS1.

We observed a visible difference in mitochondrial morphology between the control and NCS1 treated cells (Figure 2). The data produced from MitoGraph was used to create graphs in R-Studio (Figure 3). The first graph represents the total node length, the branch points and end points of the mitochondria, it is shown that NCS1 has a higher node length than the control. Nodes are the points of connection between the tubule sections of mitochondria and cross points of adjoining mitochondria. The total node length graph shows a significant increase ($p=0.0453$) between control node length and NCS1 node length. The connected components graph shows individual mitochondrion in the network. The connected components graph shows a significant increase ($p=0.0275$) in NCS1 values compared to the control. An increase in both graphs represents an increase in mitochondrial fragmentation.

MitoGraph evaluates mitochondrial fragmentation and the increase in total node length and connected components is indicative of mitochondrial fragmentation as seen with the NCS1 cells. The mitochondrial connectivity score was calculated from several parameters also generated by MitoGraph and mirrors the morphology that can be seen by eye.
The graph shows a decrease in the NCS1 connectivity score compared to the GFP connectivity score.

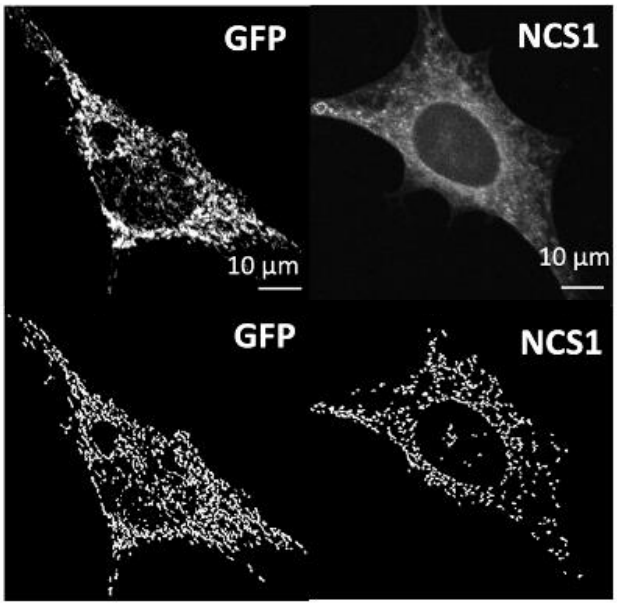

Figure 2. Image acquisition of control and overexpression of NCS1 in SMA-560 cells. (Top) original confocal imaging of GFP expressing mitochondria in control (left) and overexpressed NCS1 cells (right). Confocal images were taken using the following parameters: 60X 3X magnification, 550 HV, 2x Gain, 5% laser, and 0% offset along with a small z-spacing (0.2 um). (Bottom row) Resulting PNG images generated from original confocal images using MitoGraph. The PNG images show the mitochondrial network of the control (bottom left) and overexpression of NCS1 (bottom right). See materials and methods.

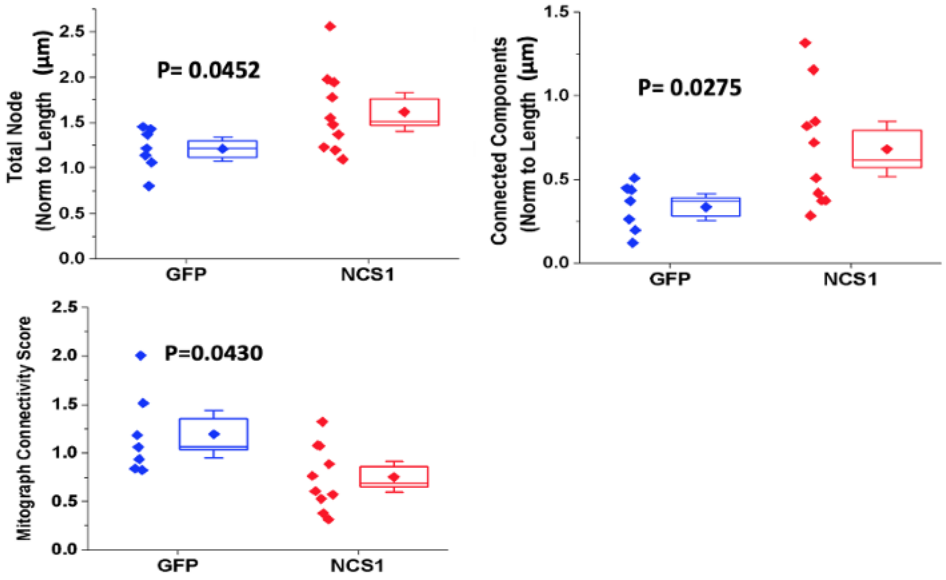

Figure 3. Graphs produced in R-Studio that represent mitochondrial morphology in control and overexpression of NCS1 in SMA-560 cells. (Top left) graph shows the total node length in the control and NCS1 cells. The total node length represents the end points and branch points of mitochondria. Higher total node length is indicative of more fragmented mitochondria. (Top right) The connected components graph represents the individual mitochondrion in the network. Higher connected component values represent less connectivity in the mitochondrial network. (Bottom) The mitochondrial connectivity score shows the connectivity in the mitochondrial network and is calculated using the PHI, AVG edge length, AVG degree, nodes, edges and connected components which are all generated from MitoGraph. [21] All of the graphs shown are statistically significant ($p<0.05$).

4. CONCLUSION

Astrocytes are vital to the human brain and are necessary for functions such as maintaining synaptic transmission, blood flow to the brain, and producing neurotropic molecules for developing and sustaining neurons. [1] Comprised of primary processes that give rise to branchlets and leaflets, known as primary astrocytic processes (PAPs), astrocytes are able to contact synapses, blood vessels, as well as other glial cells. [2] In order to transmit and receive signals, astrocytes use Ca^{2+} to communicate. Ca^{2+} is essential to astrocytes as well as its organelles, more specifically, the mitochondria. However, Ca^{2+} in mitochondrial astrocytes have been less well characterized overall compared to mitochondria in other cell types. To better understand the role of Ca^{2+} in astrocytic mitochondria, this project investigates the effects Ca^{2+} dysfunction via upregulation of NCS1, a Ca^{2+} buffering protein, will have on mitochondrial morphology and respiration.

From the experiments ran, there are definite changes in morphology and respiration due to Ca^{2+} mishandling. We hope to further our viral constructs in vivo for future reference.

The Seahorse results indicate changes in OCR and ECAR, resulting from the NCS1overexpression. The biggest changes between control cells and NCS1 cells were shown in basal respiration and ATP production. Basal respiration shows a significant increase, illustrating that initial baseline measurements are higher in NCS1 cells than in control cells. ATP production shows the mitochondria produces more ATP under NCS1 conditions than under control conditions. ATP production cannot directly be measured through the Seahorse Analyzer. However, using the Mito Stress Test Kit, oxygen consumption rate (OCR) can be used as an indirect measurement of ATP production. Basal respiration results show a significant increase

between control and NCS1 cells. This increase of OCR in basal respiration illustrates that NCS1 cells have a higher starting OCR than control cells. increase in NCS1 cells compared to control cells shows that NCS1 cells must accommodate to the cell's needs and take up more oxygen than compared to normal conditions. The ATP production significant increase in NCS1 cells illustrates the amount of ATP being produced in the electron transport chain. Both ATP production and basal respiration are higher than control cells because of the NCS1 nature of the protein. When Ca^{2+} is bound to NCS1, the mitochondria will need to transfer more Ca^{2+} in to compensate for the loss. Because Ca^{2+} plays an essential role in the production of ATP, more ATP must be generated in order to efficiently meet the cell's needs.

The results of the MitoGraph experiments show that there is a significant change ($p<0.05$) in morphology with the upregulated NCS1 compared to the control GFP. The connected components graph is used to represent the individual components rather than the entire mitochondrial network. Each connected component consists of total length, edges, and nodes. With overexpression of NCS1, there is an observable increase in total node length and connected components which means there must be a correlation between Ca^{2+} uptake and mitochondrial morphology. The mitochondrial connectivity score was calculated from several parameters also generated by MitoGraph and mirrors the morphology that can be seen by eye. The significant decrease between the control cells and the overexpressed NCS1 shows that mitochondrial health and morphology declined. After running several experiments, we can conclude that the uptake of Ca^{2+} is affected by the NCS1 protein which in turn affects the mitochondrial health.

REFERENCES

[1] Guo F, Ma J, Pleasure DE. Astrocytes. In: Aminoff MJ, Daroff RB, eds. *Encyclopedia of the Neurological Sciences (Second Edition)*. Academic Press; 2014:287-289. doi:10.1016/B978-0-12-385157-4.00172-X

[2] Santello, M., Toni, N., & Volterra,A. Astrocytes Function From Information Processing to Cognition and Cognitive Impairment. *Nature Neuroscience*, 22(2), 2019:154-166. doi:10.1038/s41593-018-0325-8

[3] Bonzano S, Crisci I, Podlesny-Drabiniok A, et al. Neuron-Astroglia Cell Fate Decision in the Adult Mouse Hippocampal Neurogenic Niche Is Cell-Intrinsically Controlled by COUP-TFI In Vivo. *Cell Reports*. 2018;24(2):329-341. doi:10.1016/j.celrep.2018.06.044

[4] Chung W-S, Allen NJ, Eroglu C. Astrocytes Control Synapse Formation, Function, and Elimination. *Cold Spring Harbor Perspectives in Biology*. 2015;7(9). doi:10.1101/cshperspect.a020370

[5] Bernardinelli Y, Muller D, Nikonenko I. Astrocyte-Synapse Structural Plasticity. *Neural Plasticity*. 2014. doi:10.1155/2014/232105

[6] Zhou B, Zuo Y-X, Jiang R-T. Astrocyte Morphology: Diversity, Plasticity, and Role in Neurological Diseases. *CNS Neuroscience & Therapeutics*. 2019;25(6):665-673. doi: 10.1111/cns.13123

[7] Chai H, Diaz-Castro B, Shigetomi E, et al. Neural Circuit-Specialized Astrocytes: Transcriptomic, Proteomic, Morphological and Functional Evidence. *Neuron*. 2017;95(3):531-549.e9. doi:10.1016/j.neuron.2017.06.029

[8] Semyanov A. Spatiotemporal Pattern of Calcium Activity in Astrocytic Network. *Cell Calcium*. 2019;78:15-25. doi:10.1016/j.ceca.2018.12.007

[9] Guerra-Gomes S, Sousa N, Pinto L, Oliveira JF. Functional Roles of Astrocyte Calcium Elevations: From Synapses to Behavior. *Frontier Cell Neuroscience*. 2017;11:427. doi:10.3389/fncel.2017.00427

[10] Khakh BS, McCarthy KD. Astrocyte Calcium Signaling: From Observations to Functions and the Challenges Therein. *Cold Spring Harbor Perspectives in Biology*. 2015;7(4):a020404. doi:10.1101/cshperspect.a020404

[11] Giorgi C, Danese A, Missiroli S, Patergnani S, Pinton P. Calcium Dynamics as a Machine for Decoding Signals. *Trends in Cell Biology*. 2018;28(4):258-273. doi:10.1016/j.tcb.2018.01.002

[12] Giorgi C, Marchi S, Pinton P. The Machineries, Regulation and Cellular Functions of Mitochondrial Calcium. *Nature Reviews Molecular Cell Biology*. 2018;19(11):713-730. doi:10.1038/s41580-018-0052-8

[13] Finkel T, Menazza S, Holmström KM, et al. The Ins and Outs of Mitochondrial Calcium. *Circulation Research*. 2015;116(11):1810-1819. doi:10.1161/CIRCRESAHA.116.305484

[14] Müller M, Ahumada-Castro U, Sanhueza M, Gonzalez-Billault C, Court FA, Cárdenas C. Mitochondria and Calcium Regulation as Basis of Neurodegeneration Associated With Aging. *Frontier Neuroscience*. 2018;12. doi:10.3389/fnins.2018.00470

[15] Shigetomi E, Saito K, Sano F, Koizumi S. Aberrant Calcium Signals in Reactive Astrocytes: A Key Process in Neurological Disorders. *International Journal of Molecular Sciences*. 2019;20(4):996. doi:10.3390/ijms20040996

[16] Nguyen LD, Nolte LG, Tan WJT, et al. Comprehensive Somatosensory and Neurological Phenotyping of NCS1 Knockout Mice. *Scientific Reports*. 2021;11(1):2372. doi:10.1038/s41598-021-81650-5

[17] Nakamura TY, Nakao S, Wakabayashi S. Emerging Roles of Neuronal Ca2+ Sensor-1 in Cardiac and Neuronal Tissues: A Mini Review. *Frontier Molecular Neuroscience*. 2019;12. doi:10.3389/fnmol.2019.00056

[18] Boeckel GR, Ehrlich BE. NCS-1 is a Regulator of Calcium Signaling in Health and Disease. *Biochim Biophys Acta Mol Cell Res*. 2018;1865(11 Pt B):1660-1667. doi:10.1016/j.bbamcr.2018.05.005

[19] Huntington TE, Srinivasan R. Astrocytic Mitochondria in Adult Mouse Brain Slices Show Spontaneous Calcium Influx Events with Unique Properties. *Cell Calcium*. 2021;96:102383. doi:10.1016/j.ceca.2021.102383

[20] Seahorse XFe96 and FXe24 Analyzers Wave 2.4 User Guide. :102.

[21] Harwig MC, Viana MP, Egner JM, et al. Methods for Imaging Mammalian Mitochondrial Morphology: A Prospective on MitoGraph. *Analytical Biochemistry*. 2018;552:81-99. doi:10.1016/j.ab.2018.02.022